



# CHORUS

This is the accepted manuscript made available via CHORUS. The article has been published as:

## Temperature dependence of spin-orbit torques across the magnetic compensation point in a ferrimagnetic TbCo alloy film

Kohei Ueda, Maxwell Mann, Paul W. P. de Brouwer, David Bono, and Geoffrey S. D. Beach

Phys. Rev. B **96**, 064410 — Published 7 August 2017

DOI: [10.1103/PhysRevB.96.064410](https://doi.org/10.1103/PhysRevB.96.064410)

# Temperature dependence of spin-orbit torques across magnetic compensation in a ferrimagnetic TbCo alloy film

Kohei Ueda<sup>\*</sup>, Maxwell Mann, Paul W. P. de Brouwer, David Bono, and Geoffrey S. D. Beach<sup>†</sup>  
*Department of Materials Science and Engineering, Massachusetts Institute of Technology,  
Cambridge, Massachusetts 02139, USA*

## Abstract

The temperature dependence of spin-orbit torques (SOTs) and spin-dependent transport parameters is measured in bilayer Ta/TbCo ferrimagnetic alloy films with bulk perpendicular magnetic anisotropy. We find that the damping-like (DL)-SOT effective field diverges as temperature is swept through the magnetic compensation temperature ( $T_M$ ), where the net magnetization vanishes due to the opposing contributions from the Tb and Co sublattices. We show that DL-SOT scales with the inverse of the saturation magnetization ( $M_s$ ), whereas the spin torque efficiency is independent of the temperature-dependent  $M_s$ . Our findings provide insight into spin transport mechanisms in ferrimagnets and highlight low- $M_s$  rare-earth/transition-metal alloys as promising candidates for SOT device applications.

<sup>\*</sup> kubond@mit.edu

<sup>†</sup> gbeach@mit.edu

In the last five years, ferromagnetic films in contact with heavy metals with strong spin orbit coupling have attracted interest for their potential utility in non-volatile random access memory elements. In these systems, current-induced spin-orbit torques (SOTs) [1,2] on the magnetization can be induced by the Rashba-Edelstein effect at the interface [3, 4] and by spin currents injected from the heavy metal due to the spin Hall effect [2, 5-26]. SOTs with both a field-like and damping-like character can manifest in such systems, with the latter capable of driving magnetization switching [1-5, 7, 9, 11-13, 15, 21, 22, 24] and magnetic domain wall motion [26-31]. SOTs have been identified and quantified by a variety of techniques including spin-torque ferromagnetic resonance [2, 7, 14, 17, 19, 25], quasistatic magnetization tilting probed through harmonic voltage measurements [6, 8-13, 17, 19-26, 28, 31] and current-induced hysteresis loop shift measurements [18, 32, 33]. Most studies of SOTs have focused on ultra-thin metallic ferromagnet/heavy-metal bilayers with interfacial perpendicular magnetic anisotropy (PMA) [1-3, 5-9, 11-13, 15-26].

Unlike ferromagnetic systems with interfacial PMA, ferrimagnetic films based on rare earth (RE)-transition metal (TM) alloys possess strong bulk PMA [31-44] as well as a low net magnetization. Moreover, the net magnetization can be tuned by the composition and temperature [32, 34-36, 38], making these materials of great interest for examining phenomena such as ultrafast optical switching [35-38], current-induced switching [39] and domain wall motion [31, 40-42] which rely on maximizing the torque exerted on the net magnetization. Since these materials consist of two magnetic sublattices whose magnetic moments possess different orbital character, their dynamics and interactions with spin currents are especially rich. Recently, SOTs in ferrimagnet/heavy-metal bi-layer films have been investigated, and the transport mechanisms were discussed [31-33, 43, 44]. Finley and Liu reported a maximum in the damping-like SOT efficiency at the smallest net magnetization in Ta/Tb<sub>x</sub>Co<sub>1-x</sub> bi-layer films

grown with a series of different compositions [32] measured at room temperature. However, a systematic temperature-dependent study of spin-transport and SOTs near the magnetization compensation temperature is lacking. For example, it is known that the anomalous Hall effect (AHE) in RE-TM alloys tracks the TM sublattice magnetization [32, 33, 44, 45], implying predominant spin-dependent interactions with the 3d orbitals as opposed to the magnetic 4f orbitals on the RE atoms. If the damping-like SOT likewise interacts predominantly with one sublattice, then the current-induced effective field should vary smoothly through the compensation temperature, whereas if it is exerted on the net magnetization, then the effective field should diverge. A temperature-dependent study can hence provide insight into the mechanisms of spin absorption in multi-sublattice systems in a single sample, in which structure, composition, and interface characteristics are fixed, and only the relative sublattice moments are tuned.

In this report, to further understand the relation between magnetic properties and spin transport mechanisms, we investigate the temperature dependence of SOTs, spin-dependent transport, and magnetic properties in a bi-layer Ta/TbCo film as temperature is swept through the magnetization compensation temperature  $T_M$ . We show that the effective field from the damping-like SOT diverges near  $T_M$ , whereas the spin torque efficiency is relatively constant with temperature. However, the coercive field also diverges near  $T_M$ , so that the switching efficiency is not expected to be enhanced. We also find that the magnitude of the AHE is relatively constant with temperature but its sign inverts at  $T_M$ , while the planar Hall effect (PHE) increases with decreasing temperature.

We fabricated the layer structure substrate/Ta(8)/Tb<sub>19</sub>Co<sub>81</sub>(6.5)/TaOx(3) by dc magnetron sputtering, where the numbers in parentheses indicate the layer thicknesses in nm. The alloy Tb<sub>19</sub>Co<sub>81</sub> was grown by co-sputtering, and the composition was estimated from the

relative deposition rates of Tb and Co. TbCo films at this composition are known to exhibit an amorphous structure [32, 34,38]. According to previous studies [32-34, 38], the magnetization of this film is expected to be Co-dominated at room temperature. The film was grown on a Ta underlayer that acts as a buffer layer and a SOT source due to the spin Hall effect [2,6,8,18, 32, 33]. The film was capped with a naturally oxidized TaOx layer to protect the TbCo film. For transport measurements, a device with a Hall cross structure, with channel dimension 10  $\mu\text{m}$  long by 5  $\mu\text{m}$  wide, was patterned by photolithography and post-deposition lift-off. Ta(3)/Au(54) contact pads were then patterned at the ends of the device for electrical measurements. Figure 1(a) shows schematically the device structure and the measurement configuration. Current was applied along the  $x$  axis and the AHE voltage  $V_{\text{AHE}}$  was measured along the  $y$  direction.  $\theta$  and  $\varphi$  represent the polar and azimuthal angles, respectively, of the applied magnetic field  $\mu_0 H$ . Temperature dependent measurements were conducted in a gas flow cryostat.

We first examined the temperature dependence of the magnetic properties. A series of out-of-plane hysteresis loops at several temperatures is shown in Fig. 1(b), measured via the AHE voltage using a standard lock-in technique. The loops all exhibit an out-of-plane easy axis consistent with PMA. With decreasing temperature, the coercivity  $\mu_0 H_c$  is found to increase and then decrease (Fig. 1(c)), at which point the sign of the AHE voltage  $V_{\text{AHE}}$  reverses. This behavior is explained schematically in Fig. 1(b). Close to  $T_M$ , the total net magnetization approaches zero since the magnetizations of two sub-lattices are equal in magnitude. At this temperature, the coercivity diverges since the torque from the applied field scales inversely with saturation magnetization  $M_s$ . The reversal of the sign of  $V_{\text{AHE}}$  is in good agreement with previous studies reporting that the AHE originates predominantly from spin-dependent interactions with the TM sublattice [32, 33, 44, 45]. From these data we estimate  $T_M \sim 200$  K, below (above)

which the Tb (Co) sublattice dominates  $M_s$ .

Figure 2(a) shows  $M_s$  versus temperature, measured with a vibrating sample magnetometer (VSM) on a companion film grown simultaneously with the patterned device. The coercivity measured by VSM corresponds closely with that measured by the AHE on the patterned device, as seen in Fig. 2(b). Finally, the perpendicular anisotropy field  $\mu_0 H_{an}$  (Fig. 2(c)) was obtained by fitting the curvature of the AHE voltage signal versus in-plane field to the Stoner-Wolfarth model to describe uniform tilting of the magnetization away from the easy axis. As can be seen, the minimum in  $M_s$  and the maximum in  $\mu_0 H_c$  and  $\mu_0 H_{an}$  all coincide.

We next examine SOTs and their variation with temperature through  $T_M$ . In order to quantify the SOT effective fields, we performed conventional harmonic voltage measurements using a lock-in amplifier [6, 8, 12]. An applied ac current causes SOTs that produce a small periodic oscillation of the magnetization about its equilibrium orientation. This generates first harmonic ( $V_{\omega 1}$ ) and second-harmonic ( $V_{\omega 2}$ ) Hall voltage signals whose in-plane field dependence can be used to quantify the effective fields corresponding to the damping-like ( $H_{DL}$ ) and field-like ( $H_{FL}$ ) SOTs.

For all temperatures,  $\mu_0 H$  was swept quasistatically between  $\pm 1.3$  T, while  $V_{\omega 1}$  and  $V_{\omega 2}$  were measured using an ac current with amplitude 1.1 mA and angular frequency  $\omega = 3.5$  kHz.  $\mu_0 H$  was applied parallel to the current direction ( $\varphi = 0^\circ$ ) to measure  $H_{DL}$  and perpendicular to current ( $\varphi = 90^\circ$ ) to measure  $H_{FL}$ . To avoid a multi-domain state, the field was oriented at  $\theta = 72^\circ$  so as to include a finite out-of-plane component. We repeated the measurements for several polar angles to verify that the results below are independent of  $\theta$  except for small (or zero)  $\theta$ , at which we observe a decreased  $V_{AHE}$  signal indicative of a multidomain state when the in-plane field component is large.

Figure 3(a) shows typical  $V_{\omega 1}$  loops at 243 K and 183 K, with field applied at  $\theta = 72^\circ$

and  $\varphi = 0^\circ$ . Figures 3 (b),(c) show  $V_{\omega 2}$  measured at these same temperatures with the field along  $\varphi = 0^\circ$  and  $\varphi = 90^\circ$ , respectively, both with  $\theta = 72^\circ$ . We find that the signs of the  $V_{\omega 1}$  and  $V_{\omega 2}$  loops invert across  $T_M$  as expected since the sign of the AHE voltage reverses [44].

Quite recently, Yu *et al.* has shown two ways for fitting  $V_{\omega 2}$ , in the low-field and high-field regimes (with respect to the anisotropy field): below  $\mu_0 H_{\text{an}}$  a linear fit is performed, whereas above  $\mu_0 H_{\text{an}}$  a parabolic fit is performed, as the magnetization tilts toward the film plane [24]. Due to the limited range of our electromagnet, the high-field regime cannot be reached for all temperatures, so we have analyzed the data in the low-field regime where  $V_{\omega 2}$  is linear, using the following relations [6]:

$$H'_{DL(FL)} = -2 \left( \frac{\partial V_{\omega 2}}{\partial H_{x(y)}} \right) \times \left( \frac{\partial^2 V_{\omega 1}}{\partial H_{x(y)}^2} \right)^{-1} - (1)$$

$$H_{DL(FL)} = \frac{H'_{DL(FL)} \pm 2\zeta H'_{FL(DL)}}{1 - 4\zeta^2} - (2)$$

Here,  $H_x$ ,  $H_y$  indicate the field components along the  $x$  and  $y$ -axes, respectively, and in Eq. (2), positive and negative signs correspond to the cases with  $z$ -component of the magnetization along  $+z$  and  $-z$ , respectively. Finally,  $\zeta$  is the ratio of planar Hall effect (PHE) and AHE coefficients  $\zeta = R_{PHE}/R_{AHE}$ ; the former was obtained by measuring the Hall voltage with the field oriented at  $\varphi = 45^\circ$  as described in Ref. [8,12,13,24]. Additionally, the anomalous Nernst effect (ANE) may give an additional contribution to  $V_{\omega 2}$  due to current-induced inhomogeneous heating [8]. We found that our sample exhibited negligible ANE contribution by measuring  $V_{\omega 2}$  at  $\theta = 0$  [8, 12].

Figure 4 summarizes the temperature dependence of the spin-transport parameters and SOT effective fields. We find that the sign of  $R_{AHE}$  reverses across  $T_M$ , whereas its magnitude varies only weakly with temperature (Fig. 4(a)), which suggests that it follows the Co sublattice magnetization, which does not change much with temperature within this range. Similarly,  $R_{PHE}$ ,

reverses sign across  $T_M$  but its magnitude does not vary considerably in this temperature range, which is reasonable since the AHE and PHE are geometrically related [45, 46].

The temperature dependence of the damping-like and field-like effective fields per unit current density, defined as  $\chi_{DL(FL)} = \mu_0 H_{DL(FL)} / J$ , are shown in Fig. 4(c) and Fig. 4(d), respectively. In computing  $\chi_{DL(FL)}$ , we estimated the current flowing in the bottom Ta layer assuming a parallel resistor model, based on the experimentally obtained resistivity of TbCo (290  $\mu\Omega\text{cm}$ ) and Ta (370  $\mu\Omega\text{cm}$ ) thin films. The fraction of current flowing through the Ta layer is estimated to be 51 % for 6.5 nm-thick TbCo and 49 % for 8 nm-thick Ta, respectively. Measurements of the device resistance and separate measurements of the sheet resistance of a thin Ta film both show a resistance change of only <2% of the measurement range, so in our calculations we assumed that the current distribution between the two layers is constant with temperature. In Fig. 4 it is seen that  $\chi_{DL}$  varies strongly with temperature and diverges near  $T_M$  where the net magnetization vanishes, consistent with previous work reported by Finley and Liu [32]. By contrast,  $\chi_{FL}$  is relatively independent of temperature (and hence  $M_s$ ), and is about an order of magnitude smaller than  $\chi_{DL}$ .

Finally, the damping-like spin-torque efficiency  $\xi_{DL}$  was calculated according to  $H_{DL}/J = \hbar \xi_{DL} / (2eM_s t_{TbCo})$  [17], where  $e$  is the electron charge,  $\hbar$  is the reduced Planck constant, and  $t_{TbCo}$  is the thickness of TbCo. Assuming the damping-like SOT derives predominantly from the spin Hall effect (i.e., neglecting contributions from an interfacial Rashba-like interaction) in the Ta layer,  $\xi_{DL}$  is related to the internal spin Hall angle  $\theta_{SH}$  of Ta and the interfacial spin transparency  $T_{int}$  through  $\xi_{DL} = \theta_{SH} T_{int}$ . The coefficient of spin transparency in a normal metal/magnetic metal bilayer can be written  $T_{int} = 2G_{eff}^{\uparrow\downarrow} / G_{NM}$ , where  $G_{eff}^{\uparrow\downarrow}$  is the interfacial spin-mixing conductance and  $G_{NM}$  is the spin conductance of

the normal metal [17]. We find  $\xi_{DL} < 0$  at all temperatures, consistent with the negative spin Hall angle of Ta [2], and that  $|\xi_{DL}| \approx 0.1$ , independent of temperature. Since the spin Hall angle of Ta has been reported to vary by less than 10% within this temperature range [15], this result suggests that the spin mixing conductance is independent of temperature despite the strong variation of  $M_s$  with temperature.

The above discussion indicates that spin-transport and SOTs show critical behaviors near the magnetization compensation temperature  $T_M$ . There is also an angular momentum compensation temperature  $T_A$ , where the angular momentum is zero although the net magnetization is nonzero, due to the different  $g$  factors of RE and TM atoms. One might expect that since the Slonczewski-like torque is framed in terms of transfer of angular momentum, that the its divergence should occur near  $T_A$  rather than  $T_M$ . Hence, our results for the SOT effective field are particularly surprising and unexpected. Previously, Stanciu *et al.* [35] and Binder *et al.* [36] have demonstrated ultra-fast switching as well as a divergence of the damping constant near  $T_A$  (not  $T_M$ ) using optical pump probe and vector network analyzer-FMR techniques. While at  $T_M$  one has  $M_{TM} = M_{RE}$ , at  $T_A$  one has  $\frac{M_{TM}}{\gamma_{TM}} = \frac{M_{RE}}{\gamma_{RE}}$  with  $\gamma_{TM(RE)} = -\frac{g\mu_B}{\hbar}$ , where  $\gamma_{TM(RE)}$  is the gyromagnetic ratio and  $\mu_B$  is the Bohr magneton and  $g$  is the Landé  $g$ -factor that accounts for the relative contribution of orbital and spin angular momentum to the total angular momentum. Based on the expression above, our TbCo composition is expected to have  $T_M < T_A$  considering the  $g$  factors of Co ( $\sim 2.2$ ) and Tb ( $\sim 1.5$ ) [47, 48] and the weak temperature dependence of the Co sub-lattice magnetization in the measurement range. The difference between  $T_M$  and  $T_A$  is  $\sim 50$  K for GdFeCo [35] and  $\sim 80$  K for GdCo [36], and our TbCo is expected to show a greater temperature difference, with  $T_A > 300$  K. Jiang *et al.* reported current-induced switching (CIS) of a spin valve system using a CoGd free layer and found that

magnetoresistance and CIS showed different temperature dependence [39], with the former showing an anomaly near  $T_M$  and the latter near  $T_A$ . Our results do not indicate any obvious anomalies in either spin transport or SOTs other than near  $T_M$ . Finley and Liu also concluded that  $\chi_{DL} \propto \frac{1}{M_s}$  based on a composition-dependence study in TbCo, [32], and suggested that past studies on ultrafast switching and CIS using conventional spin transfer torque may involve different physical mechanisms than the case of SOTs. The reasons why the current-induced effective fields track the net magnetization rather than the net angular momentum remains to be understood. Finally, we note that while this manuscript was under review, a study of temperature-dependent spin-orbit torques in Pt/GdCoFe was reported [49], which found an enhanced damping-like torque near  $T_M$ , consistent with our results.

In conclusion, we have examined the temperature dependence of magnetic properties and spin transport in bi-layer Ta/Tb<sub>19</sub>Co<sub>81</sub> films with bulk PMA. Magnetic properties vary as a function of temperature, indicating that they are dominated by the net magnetization. Despite the clear sign change of  $R_{AHE}$  as  $T$  crosses  $T_M$ , the magnitude of  $R_{AHE}$  remains almost constant, suggesting that it is related to spin-dependent interactions with the TM sublattice. By performing conventional harmonic voltage measurement, the temperature dependences of the SOT effective fields and the spin torque efficiency were quantified. It was found that  $\chi_{DL}$  is much larger than  $\chi_{FL}$  and  $\chi_{DL}$  varies inversely with net magnetization, whereas  $\chi_{FL}$  is relatively constant. By contrast, the spin torque efficiency, which accounts for the varying  $M_s$ , shows no significant temperature dependence, and since the spin Hall angle of Ta is expected to likewise vary weakly with temperature in our experimental range, the results suggest that the spin-mixing conductance does not depend on the net magnetization of the ferrimagnet. Finally, we point out that although  $\chi_{DL}$  tends to diverge near  $T_M$ , both  $\mu_0 H_c$  and  $\mu_0 H_{an}$  also diverge, which might mitigate advantages for SOT switching. Nonetheless, highly efficient SOTs in a

bulk-PMA magnetic thin films with highly tunable properties makes these materials attractive for potential device applications.

### **Acknowledgement**

We thank Dr. C. O. Avci and Prof. Chi-Feng Pai for fruitful discussion. This work was supported by the National Science Foundation under NSF-ECCS-1408172 and by the Samsung SGMI program.

### **Reference**

- [1] M. Miron, K. Garello, G. Gaudin, P.-J. Zermatten, M. V. Costache, S. Auffret, S. Bandiera, B. Rodmacq, A. Schuhl, and P. Gambardella, *Nature* **476**, 189 (2011).
- [2] L. Liu, C.-F. Pai, Y. Li, H. W. Tseng, D. C. Ralph, and R. A. Buhrman, *Science* **336**, 555 (2012).
- [3] I. M. Miron, Gilles Gaudin, S. Auffret, B. Rodmacq, A. Schuhl, S. Pizzini, J. Vogel, and P. Gambardella, *Nature Mater.* **9**, 230 (2010).
- [4] S. Emori, T. Nan, A.M. Belkessam, X. Wang, A. D. Matyushov, C. J. Babroski, Y. Gao, H. Lin, and N. X. Sun, *Phys. Rev. B* **93**, 180402 (2016).
- [5] L. Liu, O. J. Lee, T. J. Gudmundsen, D. C. Ralph, and R. A. Buhrman, *Phys. Rev. Lett.* **109**, 096602 (2012).
- [6] J. Kim, J. Sinha, M. Hayashi, M. Yamanouchi, S. Fukami, T. Suzuki, S. Mitani, and H. Ohno, *Nat. Mater.* **12**, 240 (2013).
- [7] C.-F. Pai, L. Liu, Y. Li, H. W. Tseng, D. C. Ralph, and R. A. Buhrman, *Appl. Phys. Lett.* **101**, 122404 (2012).
- [8] K. Garello, I. M. Miron, C. O. Avci, F. Freimuth, Y. Mokrousov, S. Blügel, S. Auffret, O. Boulle, G. Gaudin, and P. Gambardella, *Nat. Nanotechnol.* **8**, 587 (2013).
- [9] C. O. Avci, K. Garello, C. Nistor, S. Godey, B. Ballesteros, A. Mugarza, A. Barla, M. Valvidares, E. Pellegrin, A. Ghosh, I. M. Miron, O. Boulle, S. Auffret, G. Gaudin, and P. Gambardella, *Phys. Rev. B* **89**, 214419 (2014).
- [10] C. O. Avci, K. Garello, M. Gabureac, A. Ghosh, A. Fuhrer, S. F. Alvarado, and P. Gambardella, *Phys. Rev. B* **90**, 224427 (2014).

- [11] C.-F. Pai, M. H. Nguyen, C. Belvin, L. H. Vilela-Leao, D. C. Ralph, and R. A. Buhrman, *Appl. Phys. Lett.* **104**, 082407 (2014).
- [12] X. Qiu, P. Deorani, K. Narayanapillai, K.-S. Lee, K.-J. Lee, H.-W. Lee, and H. Yang, *Sci. Rep.* **4**, 4491 (2014).
- [13] S. Woo, M. Mann, A.-J. Tan, L. Caretta, and G. S. D. Beach, *Appl. Phys. Lett.* **105**, 212404 (2014).
- [14] T. Nan, S. Emori, C.-T. Boone, X. Wang, T.-M. Oxholm, J.-G. Jones, B.-M. Howe, G.-J. Brown, and N.-X. Sun, *Phys. Rev. B* **91**, 214416 (2015).
- [15] Q. Hao and G. Xiao, *Phys. Rev. B* **91**, 224413 (2015).
- [16] K.-F. Huang, D.-S. Wang, H.-H. Lin, and C.-H. Lai, *Appl. Phys. Lett.* **107**, 232407 (2015).
- [17] C.-F. Pai, Y. Ou, L. H. Vilela-Leão, D. C. Ralph, and R. A. Buhrman, *Phys. Rev. B* **92**, 064426 (2015).
- [18] C.-F. Pai, M. Mann, A. J. Tan, and G. S. D. Beach, *Phys. Rev. B* **93**, 144409 (2016).
- [19] K. Ueda, C.-F. Pai, A. J. Tan, M. Mann, and G. S. D. Beach, *Appl. Phys. Lett.* **108**, 232405 (2016).
- [20] M.-H. Nguyen, D. C. Ralph, and R. A. Buhrman, *Phys. Rev. Lett.* **116**, 126601 (2016).
- [21] J. Yu, X. Qiu, W. Legrand, and H. Yang, *Appl. Phys. Lett.* **109**, 042403 (2016).
- [22] M. Akyol, W. Jiang, G. Yu, Y. Fan, M. Gunes, A. Ekicibil, P. K. Amiri, and K. L. Wang, *Appl. Phys. Lett.* **109**, 022403 (2016).
- [23] M.-H. Nguyen, M. Zhao, D. C. Ralph, and R. A. Buhrman, *Appl. Phys. Lett.* **108**, 242407 (2016).
- [24] J. Yu, X. Qiu, Y. Wu, J. Yoon, P. Deorani, J. M. Besbas, A. Manchon, and H. Yang, *Sci. Rep.* **6**, 32629 (2016).
- [25] Y. Ou, C.-F. Pai, S. Shi, D. C. Ralph, and R. A. Buhrman, *Phys. Rev. B* **94**, 140414 (R) (2016).
- [26] S. Emori, U. Bauer, S. M. Ahn, E. Martinez, and G. S. D. Beach, *Nat. Mater.* **12**, 611 (2013).
- [27] K.-S. Ryu, L. Thomas, S.-H. Yang, and S. S. P. Parkin, *Nat. Nanotechnol.* **8**, 527 (2013).
- [28] J. Torrejon, J. Kim, J. Sinha, S. Mitani, M. Hayashi, M. Yamanouchi, and H. Ohno, *Nature Commun.* **5**, 4655 (2014).
- [29] K. Ueda, K.J. Kim, Y. Yoshimura, R. Hiramatsu, T. Moriyama, D. Chiba, H. Tanigawa, T. Suzuki, E. Kariyada, and T. Ono, *Appl. Phys. Express* **7**, 053006 (2014).
- [30] T. Taniguchi, K.-J. Kim, Y. Yoshimura, T. Moriyama, H. Tanigawa, T. Suzuki, E. Kariyada, and T. Ono, *Appl. Phys. Express* **7**, 053005 (2014).
- [31] D. Bang, J. Yu, X. Qiu, Y. Wang, H. Awano, A. Manchon, and H. Yang, *Phys. Rev. B* **93**, 174424 (2016).

- [32] J. Finley and Liu, Phys. Rev. Applied **6**, 054001 (2016).
- [33] K. Ueda, M. Mann, Chi-Feng Pai, A.-J. Tan, and G. S. D. Beach, Appl. Phys. Lett. **109**, 232403 (2016).
- [34] P. Hansen, C. Clausen, G. Much, M. Rosenkranz, and K. J. Witter, Appl. Phys. **66**, 756 (1989).
- [35] C. D. Stanciu, A. V. Kimel, F. Hansteen, A. Tsukamoto, A. Itoh, A. Kirilyuk, and T. Rasing, Phys. Rev. B **73**, 220402 (2006).
- [36] M. Binder, A. Weber, O. Mosendz, G. Woltersdorf, M. Izquierdo, I. Neudecker, J. R. Dahn, T. D. Hatchard, J.-U. Thiele, C. H. Back, and M. R. Scheinfein, Phys. Rev. B **74**, 134404 (2006).
- [37] C. D. Stanciu, F. Hansteen, A. V. Kimel, A. Kirilyuk, A. Tsukamoto, A. Itoh, and Th. Rasing, Phys. Rev. Lett. **99**, 047601 (2007).
- [38] S. Alebrand, M. Gottwald, M. Hehn, D. Steil, M. Cinchetti, D. Lacour, E. E. Fullerton, M. Aeschlimann, and S. Mangin, Appl. Phys. Lett. **101**, 162408 (2012).
- [39] X. Jiang, L. Gao, J. Z. Sun, and S. S. P. Parkin, Phys. Rev. Lett. **97**, 217202 (2006).
- [40] D.-T. Ngo, K. Ikeda, and H. Awano, Appl. Phys. Express **4**, 093002 (2011).
- [41] Do Bang and Hiroyuki Awano, Appl. Phys. Express **5**, 125201(2012).
- [42] T. Tono, T. Taniguchi, K.-J. Kim, T. Moriyama, A. Tsukamoto, and T. Ono, Appl. Phys. Express **8**, 073001 (2015).
- [43] Z. Zhao, M. Jamali, A. K. Smith, and J.-P. Wang, Appl. Phys. Lett. **106**, 132404 (2015).
- [44] N. Roschewsky, T. Matsumura, S. Cheema, F. Hellman, T. Kato, S. Iwata, and S. Salahuddin, Appl. Phys. Lett. **109**, 112403 (2016).
- [45] T. Okuno, K.-J. Kim, T. Tono, S. Kim, T. Moriyama, H. Yoshikawa, A. Tsukamoto, and T. Ono, Appl. Phys. Express **9**, 073001 (2016).
- [46] J. Kim, P. Sheng, S. Takahashi, S. Mitani, and M. Hayashi, Phys. Rev. Lett. **116**, 097201 (2016).
- [47] B. I. Min and Y.-R. Jang, J. Phys. Condens. Matter **3**, 5131 (1991).
- [48] J. M. D. Coey, Rare-Earth Iron Permanent Magnets (Clarendon Press, New York, 1996).
- [49] W. S. Ham, S. Kim, D.-H. Kim, K.-J. Kim, T. Okuno, H. Yoshikawa, A. Tsukamoto, T. Moriyama, and T. Ono, Appl. Phys. Lett. **110**, 242405 (2017).

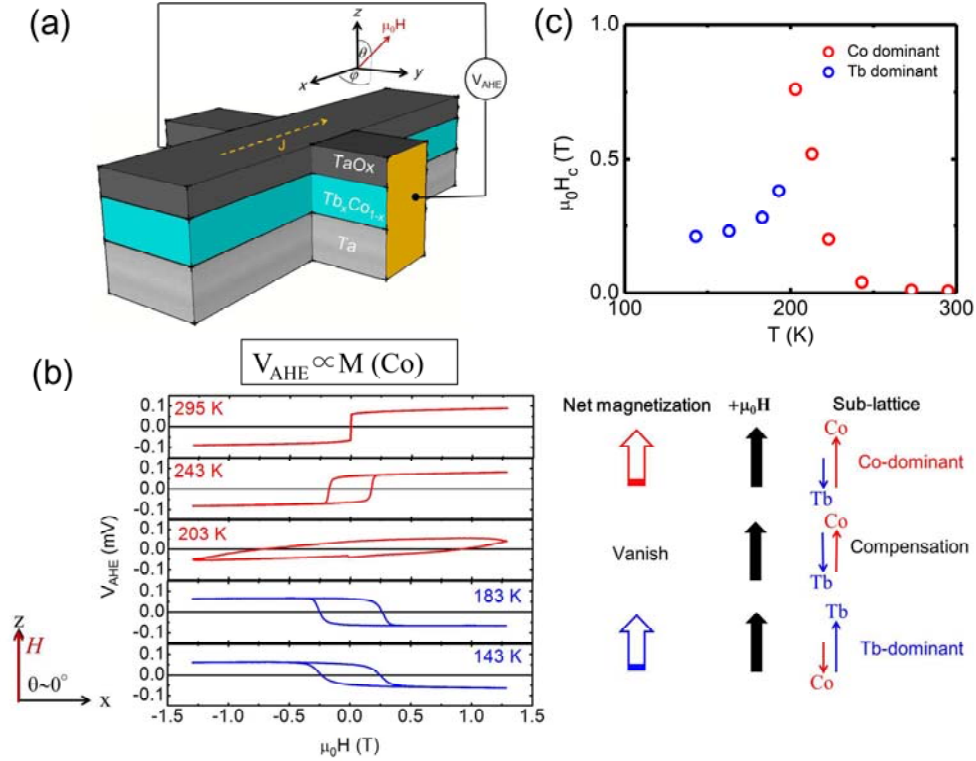


FIG. 1. (a) Schematic illustration of a device with Hall cross structure and measurement set-up. Current is applied along  $x$  axis and anomalous Hall effect (AHE) voltage is measured along  $y$  axis. (b) AHE hysteresis loops under external magnetic field  $\mu_0 H$  at polar angle,  $\theta = 0^\circ$  for various temperatures. Left sketch shows the orientation of  $\mu_0 H$ . Right sketch denotes schematically the direction of the sub-lattice magnetizations under  $\mu_0 H$  in Co or Tb dominated films. Total net magnetization vanishes when the magnetization on the two sub-lattices are equal in magnitude, defining the magnetic compensation temperature  $T_M$ . (c) Coercive field  $\mu_0 H_c$  as a function of temperature. Upon crossing  $T_M$ , the sub-lattice dominating the net magnetization transitions between Co (red symbols) and Tb (blue symbols).

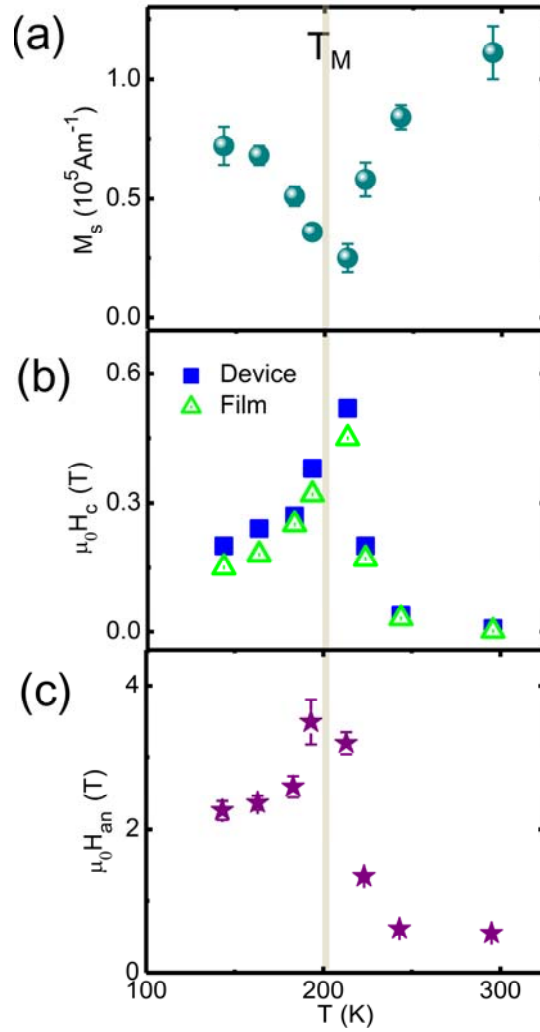


FIG. 2. Temperature dependence of (a) saturation magnetization, (b) coercivity  $\mu_0 H_c$  of patterned device and continuous film, and (c) magnetic anisotropy field  $\mu_0 H_{an}$ . Magnetization compensation temperature is marked by  $T_M$ .

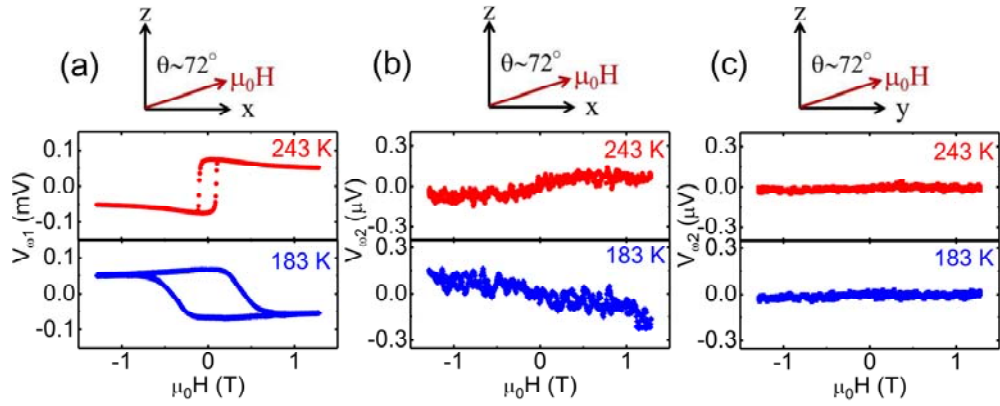


FIG. 3 (a) First and (b) second harmonic voltage response loops with  $\mu_0 H$  at  $\theta = 72^\circ$  and  $\varphi = 0^\circ$ . (c) Second harmonic voltage measurements and at  $\theta = 72^\circ$  and  $\varphi = 90^\circ$ . Sketches indicate orientation of the applied field.

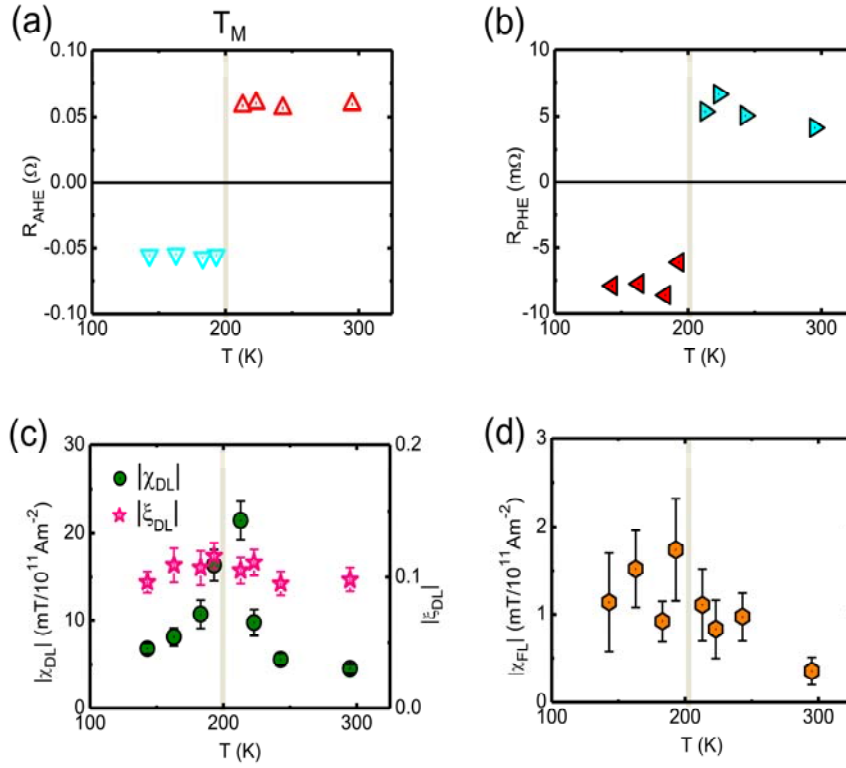


FIG. 4. Temperature dependence of (a) anomalous Hall coefficient  $R_{\text{AHE}}$ , planar Hall coefficient  $R_{\text{PHE}}$ , (c) damping-like effective field per unit current density  $\chi_{\text{DL}}$  and spin torque efficiency  $\xi_{\text{DL}}$ , and (d) effective field per unit current density  $\chi_{\text{FL}}$  from field-like torque. Gray vertical line indicates magnetic compensation temperature  $T_M$ .